Article | Received 31 October 2024; Accepted 2 March 2025; Published 11 March 2025
https://doi.org/10.55092/rl20250002

Design and fabrication of two-step expansion flexible gripper for dynamic grasping range †

Jingxiang Wang[1], Yangzesheng Lu[1], Chengqi Song[1], Bingjie Xu[2], Qinglei Bu[1,*], Jie Sun[1,*] and Quan Zhang[1]

[1] Department of Mechatronics and Robotics, Xi'an Jiaotong-Liverpool University, Suzhou, China
[2] School of AI, Suzhou Industrial Park Institute of Vocational Technology, Suzhou, China

† This manuscript is an extended version of the paper presented at the 2024 29th International Conference on Automation and Computing (ICAC) and has been granted copyright permission for publication.

* Correspondence authors; E-mails: Qinglei.Bu02@xjtlu.edu.cn (Q.B.); Jie.Sun@xjtlu.edu.cn (J.S.).

Highlights:

- A 3-finger-based flexible gripper with a curved adapter has been proposed.
- A two-step expansion control algorithm has been proposed.
- Dual air path design allows the inflatable palm and inflatable fingers to be controlled independently, ensuring a two-step expansion function.

Abstract: Recent advancements in robotics have led to the integration of flexible robotic arms into everyday applications, serving to assist or replace human operators across a variety of settings due to their safety and adaptability. This paper presents the design, simulation, and empirical evaluation of a two-step expansion flexible gripper, which incorporates inflatable fingers and a pneumatic palm to enhance grasping capabilities. The gripper operates via a pneumatic drive control system activated by a solenoid valve, allowing precise manipulation. This innovative design surpasses existing gripper configurations by facilitating the grasp of objects with diverse geometries and material properties, thereby significantly improving adaptability and functionality. This paper is an extended version of [1].

Keywords: flexible mechanical gripper; pneumatic actuation; flexible inflatable palm; 3D printing

1. Introduction

The rapid advancement of autonomous guided vehicles has garnered significant attention in the field [2,3]. These vehicles can be outfitted with robotic arms and grippers, substantially augmenting their manipulation capabilities. Various robotic arms and gripper designs have emerged, facilitating tasks such as assembly, welding, material handling, and surgical procedures, effectively serving as programmable extensions of human appendages. Furthermore, the integration of computer vision has further expanded these systems' capabilities. Advanced imaging and object recognition techniques allow for real-time monitoring and precise localization, enabling robotic arms and grippers to adapt their manipulation strategies dynamically and improve overall operational efficiency [4–6]. Traditionally, these robotic systems are constructed from rigid materials, including metals and polymers. With meticulous design, robotic arms and fingers can achieve reliable performance during specific operations, demonstrating negligible deformation under external forces. Stringent safety protocols are implemented to prevent operator exposure to potentially hazardous movements. However, these characteristics may constrain their versatility, particularly in multi-tasking environments, posing challenges in complex application scenarios.

The recent advancements in soft materials have garnered considerable interest, especially in the realm of flexible robotics, including robotic arms and grippers [7]. These soft systems typically exhibit enhanced safety compliance, particularly during human interactions. Furthermore, they show a promising capability to surpass conventional rigid robotic arms and grippers in performing tasks integral to daily life [8–10].

Soft grippers exhibit the ability to securely and reliably handle a broader range of geometries compared to conventional rigid grippers. With straightforward control strategies, these grippers can provide various grasping modes and achieve high degrees of freedom, making them particularly suitable for material handling applications. Numerous flexible robotic grippers have been conceptualized and examined, capitalizing on their advantages, such as lightweight construction, enhanced motion flexibility, and rapid responsiveness. A recent advancement by a research team resulted in the development of a novel pneumatic flexible actuator, which integrates elongation, contraction, and bending capabilities [11]. This actuator was utilized in a grasping and removal mechanism designed for effective object manipulation. Another study [12] focused on designing a gripper tailored to assist quadruped robots in safely navigating challenging environments where stability is compromised. To address the challenges of grasping delicate items underwater, researchers designed an improved flexible robotic arm incorporating mechanical sensors at its distal end [13]. This design leverages haptic feedback, enabling the inflatable fingers to execute timely action planning upon contact with an object, thus minimizing the risk of damage. This enhancement expands the applicability of robotic systems in underwater archaeology. In agricultural contexts, a flexible gripper has been explicitly proposed for harvesting and transporting thin-skinned fruits and vegetables. This system is capable of regulating interaction forces within a defined range, accommodating high acceleration while preserving the integrity of the produce [14]. Moreover, flexible robotic arms have potential applications in aerospace. One notable design mimics the trunk of an elephant, featuring eight flexible joints, resulting in an ultra-high-degreed-of-freedom system that adeptly maneuvers around obstacles [15]. This extensive operational range ensures mission success. While recent advancements have improved the perception and control capabilities of flexible fingers [16], the current requirement for manual adjustments of adapters to accommodate various finger spacings remains a constraint. This reliance on physical modifications could hinder the grippers' utility in dynamic environments, where the time and labor costs associated with frequent adjustments become significant obstacles.

Although soft grippers have progressed, their gripping capacity is still limited by the volume of their grasping workspaces and their ability to alter them for different activities. Most of the current grippers can merely grasp a single type of object, leaving the replacement of the gripper manually or the adjustment of the mechanical buckle complicated. To overcome this issue, this paper proposes a novel soft gripper with a flexible palm, which can be controlled independently to not only capture different shapes of objects but also in an adjustable dynamic grasping range based on the scale. Comprehensive extension research and functional optimisation of the proposed flexible gripper are also performed. They cover detailed modelling and calculations, introduce a novel two-step expansion control algorithm, and include simulation results for the arm's trajectory. Additionally, the complete design of the air path is provided, finite element simulation results of the adapter are added, and error bars in the experimental results are included to demonstrate consistency.

2. Robotic arm with flexible gripper

Figure 1 presents the comprehensive design framework consisting of two integral components: the robotic arm and the flexible gripper. The robotic arm's design encompasses both structural and control aspects, emphasizing stepper motor integration and trajectory planning. In the structural aspect, motor selection is based on calculations of the maximum load and subsequent strength verification to ensure optimal performance. The arm's main structure is fabricated using 3D printing technology, facilitating cost efficiency and expedited manufacturing timelines. Control of the arm is executed via stepper motors, with simulation conducted in the MOVEIT2 environment. Regarding the gripper, its design focuses on structural integrity, air path optimization, and control mechanisms to achieve versatile soft and multi-modal grasping capabilities. The gripper comprises three primary components: inflatable fingers, an inflatable palm, and an adapter. It features dual air paths: one is designated for actuating the inflatable fingers and the other is for operating the inflatable palm, thereby enhancing the grasping range. Control of these air paths is managed through solenoid valves and relays, ensuring precise operation.

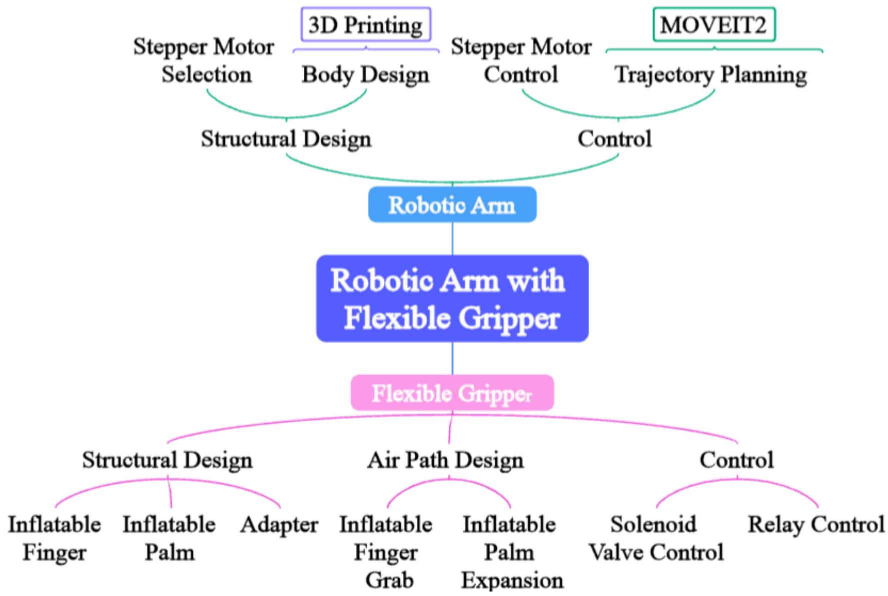

Figure 1. Design framework for the robotic arm with flexible gripper.

2.1. Robotic arm motor design

The robotic arm's design leverages the open-source framework provided by the SmallRobotArm project [17]. To enhance load capacity while minimizing reliance on metallic components, the arm's structure has been fabricated via 3D printing, significantly reducing its overall mass. The compact architecture not only minimizes spatial footprint but also enables efficient operation in confined environments such as laboratories, educational institutions, and light industrial settings. Despite its relatively small form factor, the arm boasts six degrees of freedom, affording it exceptional maneuverability. Components have been engineered with a modular approach, particularly in the joints and end-effectors, which facilitates the straightforward interchangeability of varied end-effectors (e.g., robotic claws, suction mechanisms) tailored for specific tasks. This modularity allows for the independent replacement or upgrading of components without necessitating a complete overhaul of the arm's structure.

The arm's original configuration, illustrated in Figure 2, incorporates a combination of stepper motors to actuate its six joints. Specifically, it employs two NEMA 57 stepper motors at joints 1 and 2, a NEMA 42 stepper motor at joint 3, two NEMA 28 stepper motors at joints 4 and 5, and a NEMA 20 stepper motor at joint 6. The gripper is affixed to the distal end of the robotic arm, positioned to operate with a vertical orientation. Consequently, joints 4, 5, and 6 are designated as passive joints to optimize the functionality and stability of the gripper during operation.

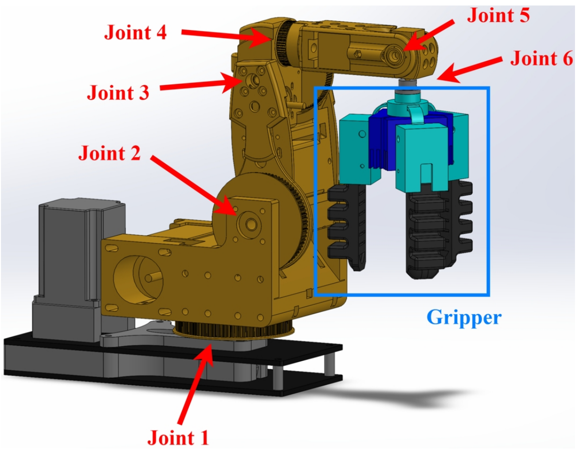

Figure 2. Modelling of six-degree-of-freedom robotic arm with the proposed flexible gripper.

The remaining three joints serve as active control elements for positioning the gripper. To establish the torque requirements for the motors associated with joints 2 and 3, calculations should be performed. For joint 2 specifically, the torque requirement is maximized when the system is in a flat lifting configuration, as this position corresponds to the longest moment arm and, therefore, the highest torque demand on the motor.

As shown in Figure 3, the target load capacity of the designed arm is $m_L = 1$ kg, and the force arm $r_L = 227.5$ mm in the lifting position. The weight of the arm assembly on top of joint 2 is $m_A = 3$ kg, and the force arm $r_A = 91.4$ mm, with gravitational acceleration $g = 9.81\ \mathrm{m/s^2}$.

The robotic arm was designed and 3D printed by our research team. "$\tau_1 = m_A g \cdot r_A$" in Figure 3 shows the gravitational torque of the robotic arm, "$\tau_2 = m_L g \cdot r_L$" shows the rated load torque of the robotic arm, and "$\tau_j = m_A g \cdot r_A + m_L g \cdot r_L$" means that the torque of the selected motor should be torque balanced with the sum of the gravitational torque and rated load torque of the robotic arm. These are the selection and calibration criteria of the motor used in the design of the robotic arm. The motor can make the robotic arm work properly after the selection. Based on these key values, the static torque τ_j that needs to be supplied to the joints during the lifting position can be briefly calculated. The specific calculation is listed as follows:

$$\tau_j = m_L g \cdot r_L + m_a g \cdot r_A = 4.922 N \cdot m \tag{1}$$

The synchronizing wheel of the motor transmits motion to the follower wheel via a timing belt, facilitating the rotation of joint 2. In this analysis, we will ignore losses attributed to friction and other factors and will perform our calculations without accounting for transmission efficiency. The gear ratio between the driving wheel and the follower wheel is 24:160, allowing us to calculate the continuous torque τ_c that the motor must deliver to maintain the robotic arm in a horizontal position.

$$\tau_c = \frac{24}{160} \cdot \tau_j = 0.7383 N \cdot m \tag{2}$$

As a rule of thumb in practice, to lift the arm from the static position, the motor must provide a starting torque of approximately 2 times the static torque τ_c.

$$\tau_s = 2\tau_c = 1.4766 N \cdot m \tag{3}$$

Due to the inherent limitations of stepper motors in delivering peak torque, the peak torque requirement for the motor, denoted as τ_s, should effectively be considered as the rated torque requirement. Consequently, for Joint 2, it is necessary to select a motor with a minimum rated torque of approximately 1.5 N·m. This approach will be applied to determine the specifications for the remaining joints, ensuring each is matched to its corresponding torque requirements in a similar, methodical manner.

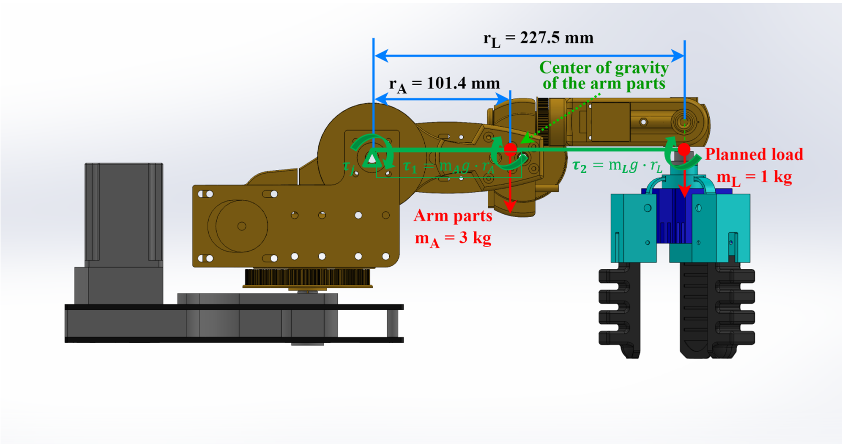

Figure 3. Key parameters of the torque balance of the robotic arm.

2.2. Robotic arm control

To implement robotic arm control, this work leverages the MoveIt2 framework within the ROS2 ecosystem to facilitate motion management. MoveIt2 encompasses a comprehensive functional package that supports various capabilities, including collision detection, manipulation control, motion planning, 3D sensing, kinematics, and more. It serves as an efficient platform for developing robotic applications, assessing designs, and enabling architectural integration within robotics environments. Figure 4 illustrates the motion planning process for the robotic arm model utilizing the MoveIt2 package. In the process of motion planning for a robotic arm model using MoveIt2, the URDF model of the robotic arm needs to be loaded and configured with the appropriate kinematic parameters first. Then, the working environment is established using MoveIt2's visualization tool, RViz2, with obstacles and other environmental information considered in the planning. Next, built-in planners such as OMPL are used to generate motion paths that satisfy joint constraints and collision detection requirements, and the paths are optimized to ensure that the planning results are safe and efficient. Finally, the generated trajectories are passed to the robot arm through the control interface for path tracking and execution, and the motion status is monitored in real time to make necessary adjustments.

For enhanced motion planning in RViz, it is crucial to localize objects accurately. The coordinates of any point Q on a rigid body can be represented in multiple coordinate systems using vectors and direction cosines. The transformation between these coordinate representations can be described mathematically as follows:

$$x = x' \cos(x,x') + y \cos(x,y') + z' \cos(x,z') \tag{4}$$

$$y = x' \cos(y,x') + y \cos(y,y') + z' \cos(y,z') \tag{5}$$

$$z = x' \cos(z,x') + y \cos(z,y') + z' \cos(z,z') \tag{6}$$

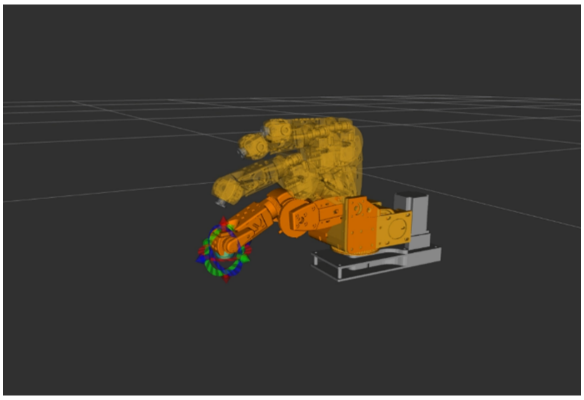

Figure 4. Kinematic simulation of the robot arm via Moveit2 in ROS2.

The direction cosine matrix (DCM) serves as a critical tool for characterizing the directional relationship between two coordinate systems. The transformation equations (4), (5), and (6) facilitate the conversion from one coordinate frame to another. Specifically, coordinates x', y', and z' represent the position of point Q in the original coordinate system, while x, y, and z denote its position in the target coordinate system. In the context of trajectory planning with MoveIt 2, the precise position and orientation of the end-effector are paramount. The application of a DCM allows for the conversion of the end-effector's local coordinates and orientation to a global reference frame, such as the world coordinate system. This matrix enables accurate computations of the position and orientation of individual components of the robotic arm in global space. Furthermore, as the flexible robotic arm executes designated tasks, its kinematic model is concurrently simulated within the Rviz platform, providing real-time visualization and validation of the arm's movements and orientations in the context of its operational environment.

2.3. Flexible gripper design

2.3.1. Working principle and proposed two-step expansion algorithm

The primary structure of the flexible gripper consists of three inflatable fingers, an inflatable palm, and an adapter, as illustrated in Figure 5. The inflatable palm and inflatable fingers are controlled by separate air paths. The flexible gripper's first expansion function is realized by the inflatable palm, and the flexible gripper's second expansion function is realized by the inflatable fingers. The adapter is a connecting component that connects the inflatable palm and the inflatable fingers.

When the flexible gripper grasps the target object, it will judge the maximum radius of the target object to ensure that the air pressure control fingers are adjusted to the correct grasping range. There are four cases when a flexible gripper grasps an object:

(a) Case 1: Grasp an object without using the expansion.
(b) Case 2: Grasp an object using only the first expansion.
(c) Case 3: Grasp an object using both the first and second expansions.
(d) Case 4: Grasp an object using only the second expansion (Support an object internally).

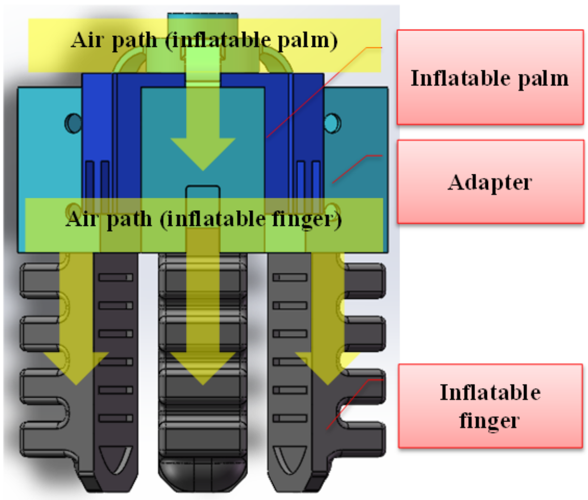

Figure 5. Key structure of the flexible gripper: Inflatable palm, adapter, and inflatable fingers.

The inflatable palm's inflation realizes the first expansion, and the inflatable fingers' inflation realizes the second expansion. The expansion of the flexible gripper is not activated in Case 1. In Case 2, the first expansion of the flexible gripper is activated, and the second expansion is not activated. In Case 3, both the first and second expansions of the flexible gripper are activated. As the size of the target objects increases, Cases 1–3 will be applied accordingly. The internal support function of the flexible gripper is activated in Case 4 through merely a second expansion. Table 1 shows the proposed two-step expansion control logic.

The inflatable palm's expansion is simulated and monitored to ensure accuracy across different pressure settings. The correlation between the palm's inflation and the finger's extension is tested both in simulation and experiments. As illustrated in Figure 6, when the flexible gripper receives a grasp signal, it derives the approximate size of the target object through the visual recognition of the camera and executes the appropriate grasp case method according to the size of the target object. There are four types of grasp cases, each grasp case corresponds to a different target object size. The purple path indicates the usage of the flexible gripper for the inflatable palm and inflatable fingers in Case 3. Finally, the functions of the flexible gripper to hold the target object are all realized by the inflation or deflation of the inflatable fingers.

Table 1. Proposed two-step expansion control logic.

Case number	Palm expansion(first expansion function)	Fingers expansion(second expansion function)
Case 1	N	N
Case 2	Y	N
Case 3	Y	Y
Case 4	N	Y

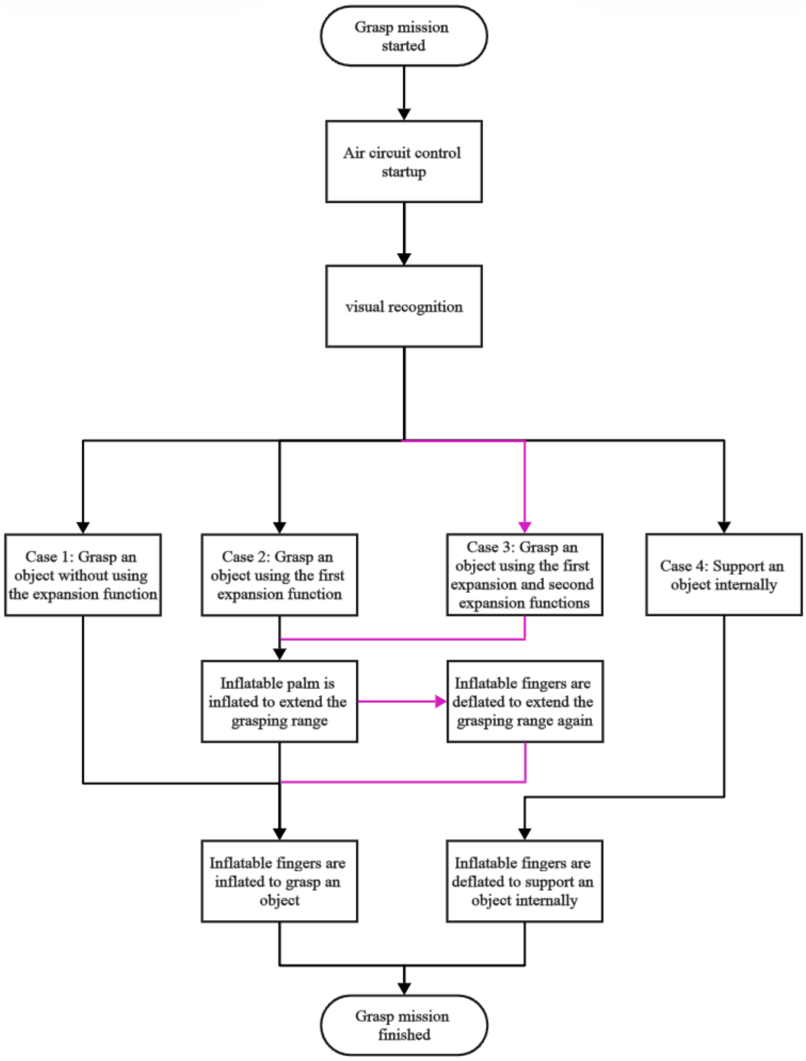

Figure 6. Flowchart of the flexible gripper control strategy.

Figure 7 shows the operating principle of controlling the position of the inflatable fingers by pneumatically actuating the inflatable palm. The key positional points of the flexible gripper are marked. *A* is the top centre connection point of the adapter, *B* is the fingertip of the inflatable finger, *C* is the horizontal centre point of the three fingertips, B' is the bottom midpoint of the inflatable palm side, and C' is the centre point of the inflatable palm bottom. Triangle ABC and triangle $AB'C'$ are a pair of similar triangles ($\triangle ABC \sim \triangle AB'C'$); the similarity ratio is 3:1.2 ($\propto = 3:1.2$), so the lengths of BC and $B'C'$ have a proportional relationship. By controlling the expansion function of the inflatable palm, the length of $B'C'$ can be controlled, and then the length of BC can be controlled, and the first expansion range of the flexible gripper can be precisely controlled by this method. The second expansion range of the flexible gripper can be determined by controlling the pressure inside the fingers and the material's ductility.

ΔL is the finite element simulation value. As shown in Figure 8, it is the maximum combined displacement of the inflatable palm.

$B0'C0'$ is the original radius of the flexible gripper when it is not expanded.The simulation values $B'C'$ and BC are given by:

$$B'C' = \Delta L + B0'C0' \tag{7}$$

$$BC \propto B'C' \tag{8}$$

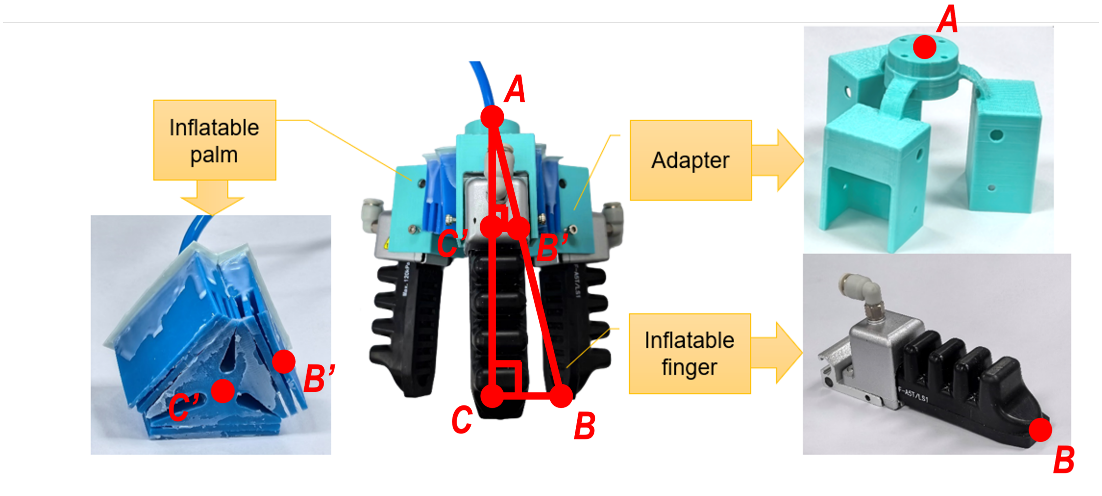

Figure 7. Geometrical modeling of grasping range. There is a proportional relationship between the expansion range of the inflatable palm and the grasping range of the inflatable fingers.

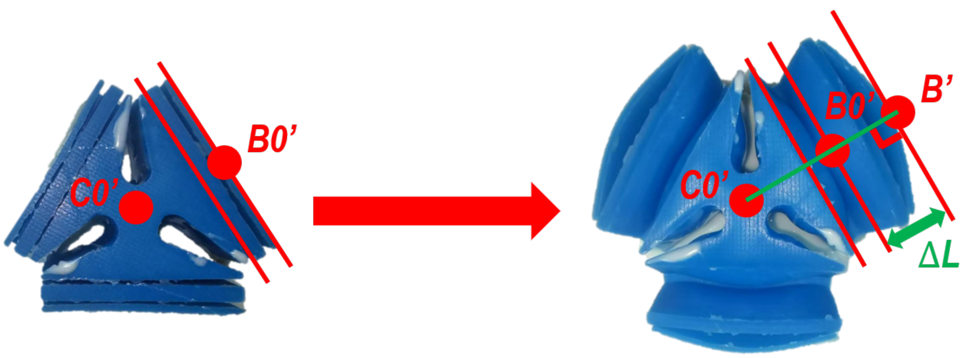

Figure 8. Overall displacement of inflatable palm. Changes in maximum displacement before and after expansion of the inflatable palm are shown.

Table 2 provides the maximum deformation and expansion parameters of the inflatable palm and the corresponding grasping radius of the flexible gripper under various air pressures.

Table 2. Simulation and experimental results of deformation and key parameters of inflatable palm with different air pressure.

Pressure value (kPa)	Maximum palm deformation (mm) $\triangle L$	$B'C'$ (mm) (Simulation)	$B'C'$ (mm) (Experiment)	BC (mm) (Simulation)	BC (mm) (Experiment)
0	0	9.75	9.75	24.37	24.55
25	7.68	17.43	17.96	43.57	44.90
30	8.47	18.22	18.90	45.55	47.25
35	9.16	18.91	19.11	47.27	47.78
40	9.75	19.50	19.78	48.75	49.45
45	10.28	20.03	20.33	50.07	50.83
50	10.50	20.25	20.77	50.62	51.93
55	11.20	20.95	21.18	52.37	52.95
60	12.61	22.36	23.56	55.90	58.90
65	13.99	23.74	24.91	59.35	62.28
70	15.34	25.09	26.34	62.72	65.85
75	15.67	27.45	28.59	68.55	71.48

2.3.2. Theoretical analysis of inflatable palm

When air pressure is increased inside a deformable, thin-walled air chamber, the imbalance in pressure between the inside and outside causes the chamber to deform. Specifically, for the inflatable palm, the chosen silicone material exhibits linear elastic deformation and is isotropic. According to Hooke's law, there is a linear relationship between stress and strain:

$$\sigma = E \cdot \varepsilon \tag{9}$$

where σ is the stress, E is the elastic modulus of the material, and ε is the strain. Thus, the air room deformation is calculated as follows:

$$\varepsilon = \frac{\sigma}{E} \tag{10}$$

In a homogeneous thin-walled air chamber, the internal pressure p induces stresses on its surface. These stresses can be classified based on their direction of action into circumferential stress along the surface and axial stress perpendicular to the surface.

$$\sigma_\theta = \frac{p \cdot r}{t} \tag{11}$$

$$\sigma_x = \frac{p \cdot r}{2t} \tag{12}$$

Where σ_θ is the annular stress, σ_x is the axial stress, p is the pressure inside the air room, r is the mean radius of the air room, and t is the wall thickness. Thus, the strain equation in different directions can be further expressed as:

$$\varepsilon_\theta = \frac{p \cdot r}{E \cdot t} \tag{13}$$

$$\varepsilon_x = \frac{p \cdot r}{2E \cdot t} \tag{14}$$

Where ε_θ is the annular strain, ε_x is the axial strain.

According to the equations, the annular strain occurring in the thin-walled air chamber is significantly larger than the axial strain under the same boundary conditions. The elastic modulus, denoted as E, also plays a crucial role in influencing the amount of strain due to the varying magnitudes of the different variables involved. The design of the inflatable palm allows its outer surface to expand during inflation, resulting in an inclined surface that helps turn the fingers outward. To achieve this design goal, it is essential to analyze and adjust the expansion rate for each part of the inflatable palm. Altering the structure and material distribution of the palm can accomplish this. By doing so, the inflatable palm can be directed to turn in a specific direction when air pressure is applied.

To enhance the horizontal expansion of the outer structure, as illustrated in Figure 9, it is essential to permit maximum annular strain in the horizontal direction. Concurrently, the air chamber at the top is divided into continuous gully segments. When air pressure is applied, the annular strain generated on the horizontal surfaces at both ends causes the air walls on either side to tilt. This annular strain includes a horizontal component, which influences the horizontal deformation of the inflatable palm.

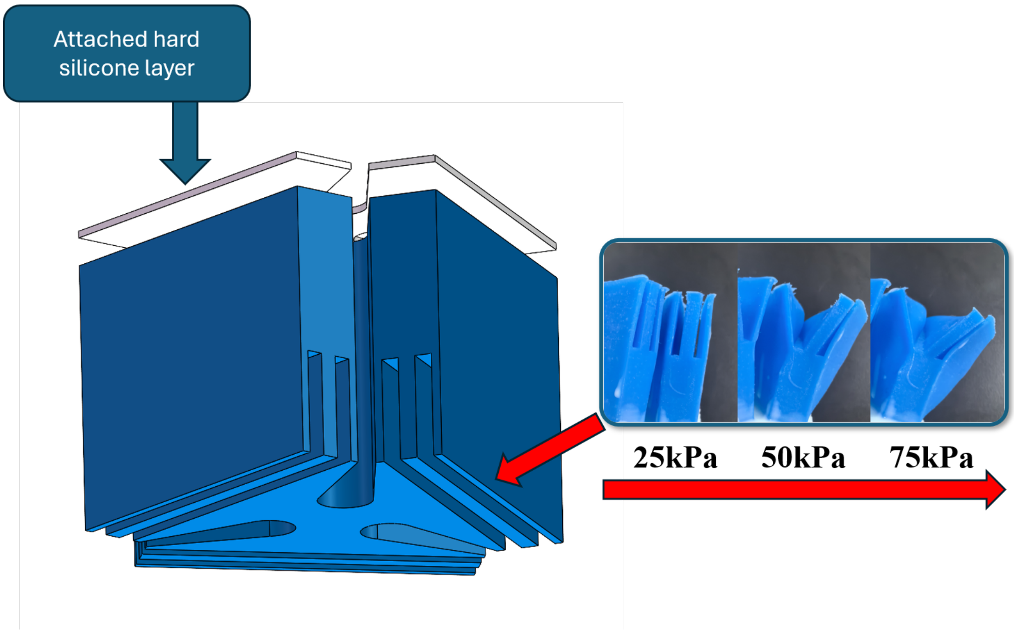

Figure 9. Structure design of inflatable palm with its expansion under different air pressure.

Furthermore, a hard silicone material, Smooth-960, is attached to the bottom of the inflatable palm. This material has a high elastic modulus, which significantly restricts the deformation of the bottom of the inflatable palm when air pressure is applied. By increasing the elastic modulus E, the annular deformation is minimized. By adjusting the expansion rates of the top and bottom sections, significant differences in their deformation under the same air pressure can be achieved. This discrepancy allows the outer surface of the inflatable palm to maintain a controlled inclination, and the resulting deformation applies pressure to the adapter, facilitating the movement of the fingers.

2.3.3. Production of flexible gripper

The flexible gripper's primary architecture comprises three inflatable fingers, an inflatable palm, and a connector adapter. The inflatable fingers, constructed from soft rubber, facilitate bending and deformation, which is crucial for effective object grasping. The inflatable palm is designed to inflate in a specific direction, thereby enhancing the overall grasping capability. Unlike conventional fixed grippers, the adapter has been innovatively redesigned in this study to allow for a dynamic gripping range, acting as a critical intermediary between the inflatable fingers and the palm. For the fabrication of the inflatable palm, silicone materials Mold Star 30 and Smooth-Sil 960 are employed. Molds for the components are produced via 3D printing, followed by a molding process to create the final gripper components.

The fabrication process for the flexible inflatable palm is depicted in Figure 10. Each mold component is designed with a centrally symmetrical cross-section, ensuring all parts share a coincident central axis. The inclusion of three positioning holes, aligned within the same plane, allows for precise positioning of the components, thus guaranteeing axial alignment. These multiple positioning holes also maintain a uniform wall thickness throughout the mold, critical for preserving the desired mechanical properties. Once the molding material is introduced into the assembled mold, it undergoes solidification, resulting in a capped inflatable palm with an unsealed bottom. To create a fully enclosed cavity, an additional sealing process is necessary to close the body of the inflatable palm.

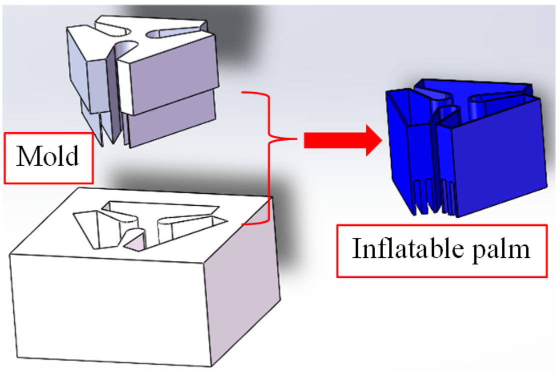

Figure 10. Mold design of the inflatable palm. The main part of the inflatable palm is made by mould release.

To enhance the grasping range of the flexible gripper, the inflatable palm is designed to expand through the application of air pressure. This expansion induces surface deformation in the adapter, further increasing the distance between the inflatable fingers and the center of the gripper. To optimize this expansion process, the adapter incorporates a curved structural design, as illustrated in Figure 11. The simulation results for various thicknesses of this curved structure are detailed in Table 3, where displacement indicates the increase in the adapter's radius under specific load conditions. $N.A.$ reflects a broken connection. Analysis reveals that the primary cause of these failures is stress concentration occurring in localized regions of the adapter. When loads are unevenly distributed, localized stresses can significantly exceed the average, leading to rapid strain increases that surpass the material's yield strength. This results in plastic deformation and a gradual decline in load-bearing capabilities. Under elevated loads or fatigue, cracks may initiate and propagate from these stress concentration zones, ultimately resulting in the catastrophic failure of the adapter. Furthermore, the integrity of these regions is compromised by the stress concentrations, elevating the likelihood of damage even when the overall structure appears intact. For instance, at a thickness of 2 mm, the curved design allows the adapter to achieve substantial deformation with minimal pressure application—applying a stress of 5 N yields an extension of 11.7 mm in the gripper's radius. Simultaneously, this curvature mitigates damage, effectively dispersing stress concentrations within the structure.

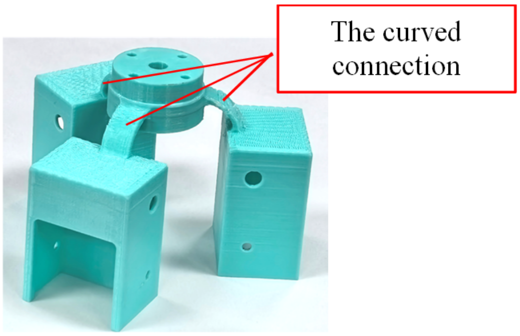

Figure 11. 3D printed adapter with curved connection. The curved connection is the area of stress concentration.

Table 3. Thickness optimization for the adapter's curved structure.

Thickness	1 mm			
Simulated Force	1 N	3 N	5 N	7 N
Expansion	28.56 mm	*N.A.*	*N.A.*	*N.A.*
Thickness	2 mm			
Simulated Force	1 N	3 N	5 N	7 N
Expansion	2.38 mm	7.10 mm	11.71 mm	16.14 mm
Thickness	3 mm			
Simulated Force	1 N	3 N	5 N	7 N
Expansion	1.04 mm	3.12 mm	5.19 mm	7.24 mm

2.4. Air path control design

The pneumatic air delivery system for the designed gripper consists of two distinct sections to regulate the inflatable palm and fingers. The air supply configuration for the inflatable fingers features components similar to those shown in Figure 12(a). However, it necessitates a negative pressure condition, thus requiring an additional pathway as illustrated in Figure 12(b). In Figure 12(a), the red-delineated air route denotes the positive pressure needed for gripping operations. Conversely, the blue-marked air route in Figure 12(b) is activated to induce a reverse bending state in the inflatable fingers through the application of negative pressure, facilitating internal support for objects such as containers and boxes.

The inflatable finger mechanism is engineered to facilitate airflow control for object manipulation and internal support. Key components of this system include an air pump, air filter, solenoid valve, pressure regulator, and a flexible gripper. Upon activation of the solenoid valve, the air chamber undergoes a transition that opens a pathway to allow positive air pressure to enter the system. The pressure regulator subsequently calibrates the air pressure to the specified operational level. This pressure differential induces airflow into the inflatable finger, resulting in bending as internal pressure escalates. Through this bending motion, the finger is capable of securely grasping the target object. Once the regulator stabilizes the pressure at the designated working level, continuous airflow further inflates the finger, enhancing its downward bend due to increased internal pressure. When the air pump is deactivated, the system's pressure normalizes to atmospheric levels, leading to air expulsion through the muffler plug integrated into the solenoid valve. Consequently, the object is released, allowing it to descend under gravity, and the finger reverts to its original form as the bending deformation dissipates.

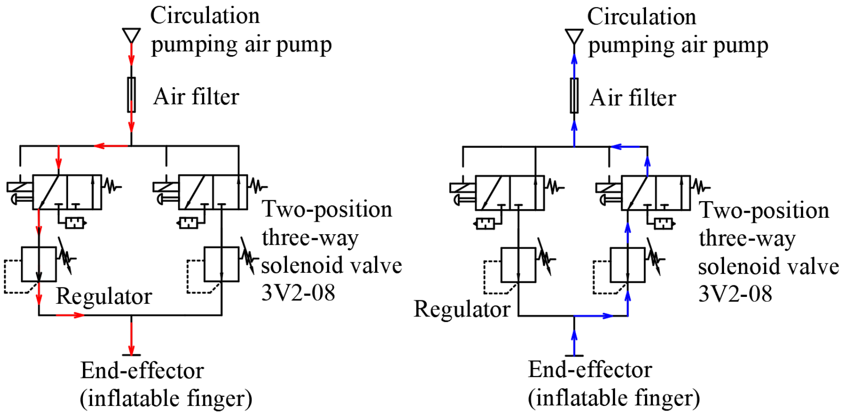

Figure 12. Air path design of inflatable fingers. **(a)** Positive pressure environment air path design and gas flow direction. Gas is routed by the red line from the pump through the gas filter, solenoid valve, regulator and finally to the end-effector (inflatable finger); **(b)** Negative pressure environment air path design and gas flow direction. The gas is pumped from the blue line by a gas pump.

Simultaneously, the air path control design of the inflatable palm uses the component connection method of "air pump - air filter - solenoid valve - regulator - inflatable palm". When the air source is activated, the air enters the air path, and the air filter cleans the air. When the solenoid valve is energized, the left air chamber replaces the right air chamber in the air path, and the left air path is opened. When the size of the object being grasped by the flexible gripper exceeds the maximum grasping range of the inflatable fingers, the ability of the inflatable palm and adapter to expand in a specific direction can enhance the grasping range of the flexible gripper. Figure 13 illustrates a diagram of the air path of the inflatable palm expanding in the intended direction in a positive pressure environment.

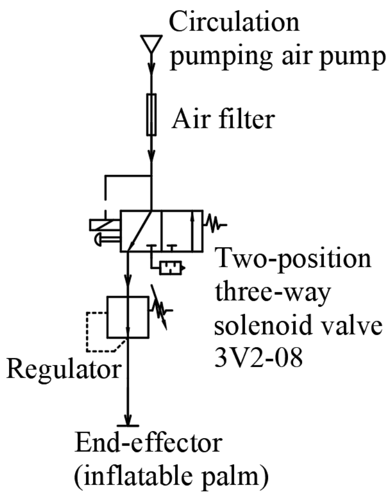

Figure 13. Air path design of inflatable palm.

3. Simulation and experimental results

3.1. Inflatable palm and finger

The simulation experiment for the flexible gripper encompasses an analysis of the expansion ranges of both the palm and fingers under various pressure conditions. The objective of this simulation is to evaluate the viability of the proposed designs. To enhance the design of the inflatable palm and fingers, we employed finite element analysis (FEA) to assess the necessary kinematics and deformation characteristics. This approach builds upon a previously established finger design [18]. However, in this study, we have modified the geometry and internal architecture of the finger to align with the manipulation requirements of our robotic system.

When the solenoid valve is activated to connect with the air supply, air enters the chamber, resulting in the expansion of the inflatable palm in a predetermined direction. The simulation results depicted in Figure 14 illustrate the displacement gradient across the structure of the inflatable palm under an applied pressure of 50 kPa. The accompanying legends specify displacement values (notated as URES, in mm), indicating the degree of deformation experienced by various structural components. The color scale corresponds to the range of displacements observed. At the dome's apex, displacement values approach approximately 10.6 mm, indicating significant deformation driven by the internal pressure exerting an outward force. In contrast, the base of the palm exhibits minimal displacement, effectively anchoring the structure and maintaining stability. The simulation data confirms that the outer surface of the inflatable palm can be dynamically deformed toward the targeted direction under positive pressure, facilitating the finger-flipping mechanism. Notably, the displacement increases progressively from the outer edges of the inflatable palm toward the central region, ultimately reaching the material's deformation limits. This controlled performance under pressure highlights the effective design and functionality of the inflatable palm structure.

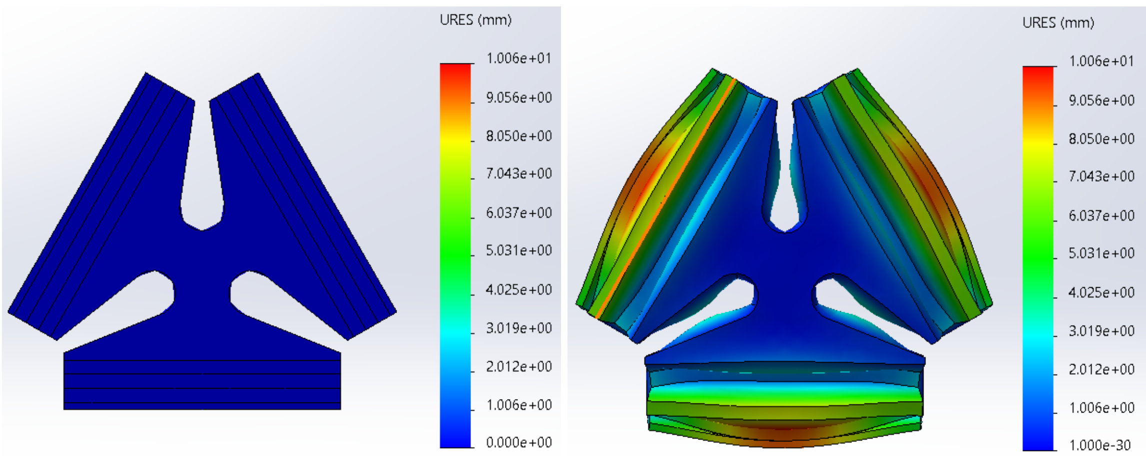

Figure 14. Simulation results of inflatable palm. **(a)** The initial state when the inflatable palm does not start to inflate; **(b)** The maximum displacement of the inflated palm was 10.6 mm at 50 kPa.

As demonstrated in Table 4, Mold Star 30 allows a maximum palm deformation of 10.5 mm at a standard pressure of 50 kPa. This deformation is significant compared to Nylon, which only deforms by 0.57 mm under the same conditions, illustrating that materials with high stiffness (like Nylon) provide insufficient flexibility, resulting in minimal deformation. This rigidity hinders the gripper's ability to adapt its shape to grasp various objects effectively. $N.A.$ indicates that the hydrogel cannot stand the air pressure of 50 kPa, resulting in breakage. Compared with hydrogel, Mold Star 30 has soft characteristics, while its toughness can also support it in completing the elastic deformation.

Table 4. Maximum deformation of inflatable palms under different materials at 50 kPa.

Material name	Maximum palm deformation (mm)
Mold star 30	10.5
Nylon	0.57
Hydrogel	$N.A.$

Figure 15(a) shows the simulation result of a deformed inflatable finger under 75 kPa positive pressure. The tip of the inflatable finger showed the most significant displacement, approximately 14.88 mm, which indicates that this component stretched considerably when it was pressurized. The displacement gradient decreases toward the base, which remains more stable and experiences far less stretching. This deformation pattern underlines the differential response of the finger's segments to internal pressure, indicating that the inflatable finger can satisfy a reliable connection of its base to an adapter and still have a sizable amount of deformation at its tip.

The deformation characteristics of the inflatable finger under negative pressure are depicted in Figure 15(b). Operating at a negative pressure of 0.5 atmospheres results in a peak displacement of 26.31 mm at the pneumatic finger's tip. This pronounced inward movement signifies a substantial compressive force, leading to the collapse of the tip inwards.

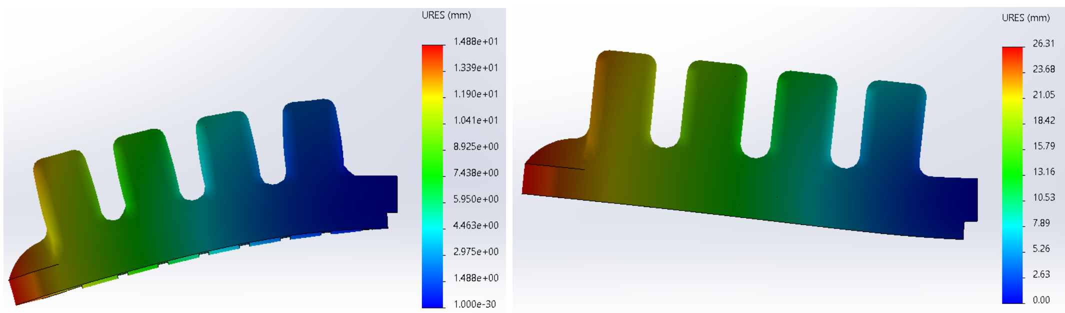

Figure 15. Simulation results of the inflatable finger. **(a)** The maximum displacement was 14.88 mm at a positive pressure of 75 kPa; **(b)** The maximum displacement was 26.31 mm at a negative pressure of 0.1 atmosphere.

In Figure 16, we present the finite element analysis conducted on the adapter fabricated from 3D-printed ABS material. The simulation aims to evaluate the structural integrity of the adapter under load. Notably, the maximum displacement observed is 11.71 mm at a thickness of 2 mm for the adapter's curved design. Importantly, the adapter withstands this level of deformation without succumbing to stress concentrations, thereby fulfilling the operational requirements for the flexible gripper's object manipulation capabilities.

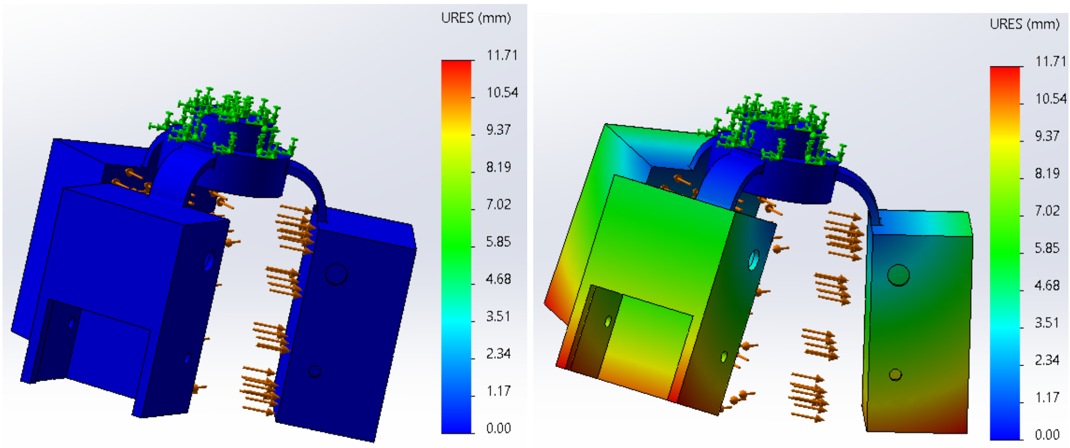

Figure 16. Finite element simulation and analysis experiment of adapter. **(a)** The initial state when the adapter is not forced; **(b)** The maximum displacement was 11.71 mm under a force of 5 N.

3.2. Preliminary test of flexible gripper

Figure 17, showcasing the palm inflated and expanded multiple times in a controlled setting, reflects minimal measurement variability. This consistent repeatability is crucial as it substantiates the reliability of the inflatable palm for practical applications, ensuring that the device performs predictably under different conditions.

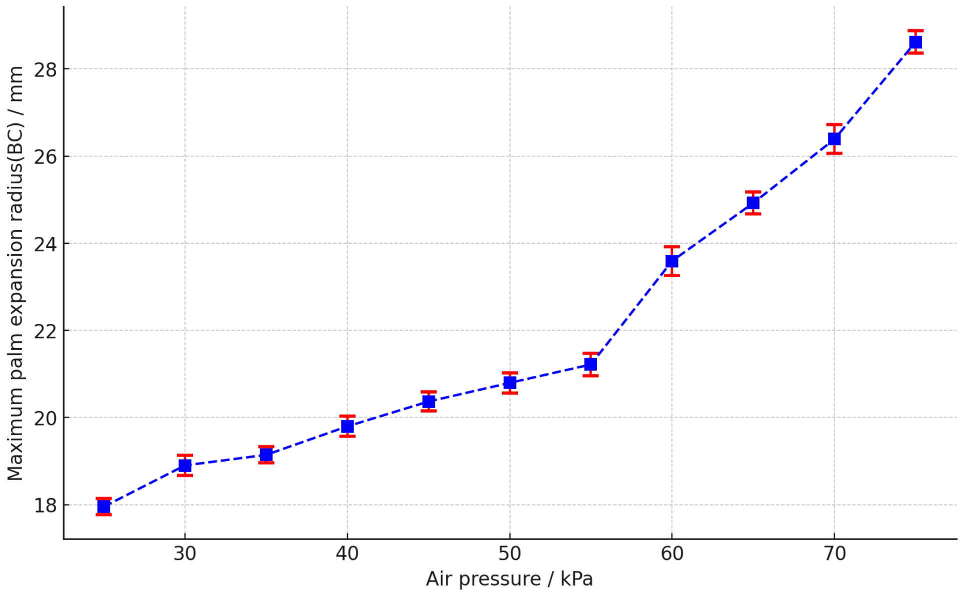

Figure 17. Error bar of the grasping radius at different air pressures caused by inflatable palm expansion.

Figure 18 depicts the comparison between the simulation and experimental results of the inflatable finger under varying air pressures. Points 1-5 are located at the same horizontal distance, while point 6 is positioned at the tip of the inflatable finger, exhibiting different vertical and horizontal distances compared to the other points. As a result, the variation in the X and Y positions of point 6 is smaller than that of the other points. *L* represents the length of the inflatable finger. This figure shows the consistency and effectiveness of the fingers' variation.

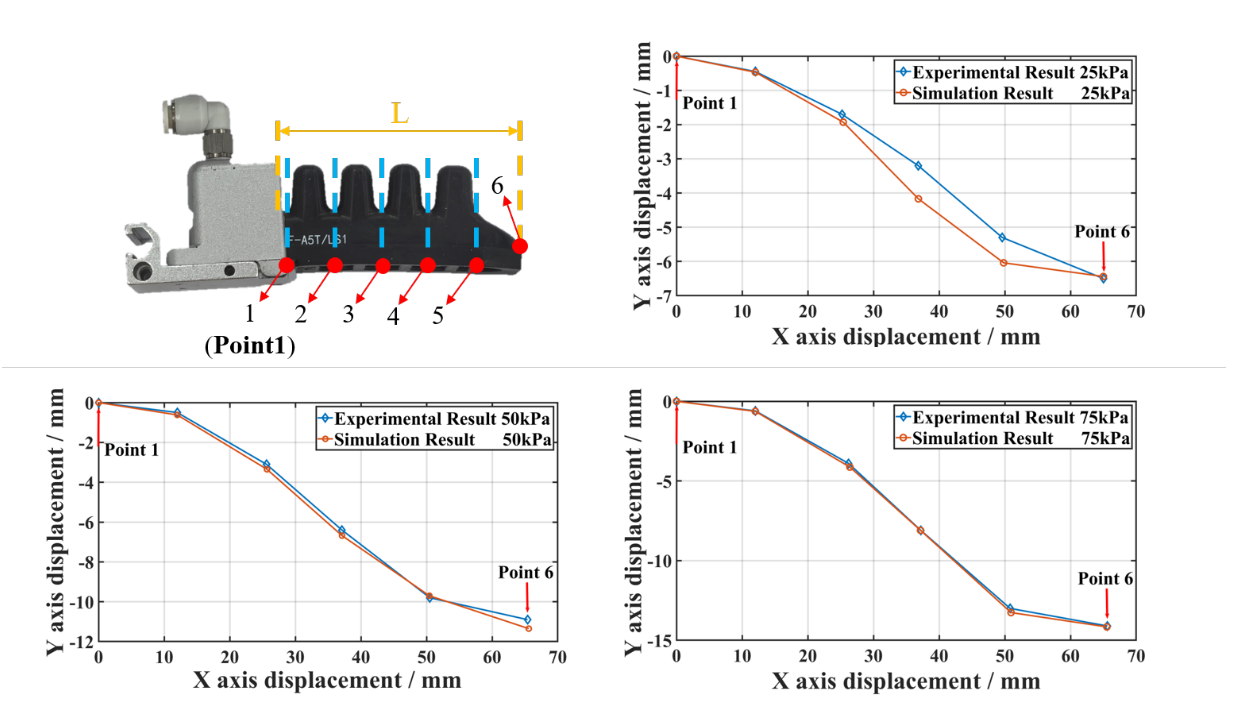

Figure 18. Simulation and experimental results of inflatable finger under different pressure.

The differences at lower pressures primarily result from simulation limitations and visual exaggeration in the graph. Simulations use simplified material models and geometries to reduce computational complexity, which may not fully capture real-world variations caused by material imperfections, manufacturing inconsistencies, or environmental factors. Additionally, the scaling of the y-axis in Figure 18 visually amplifies discrepancies, but the actual maximum deviation is only about 1mm (approximately 8% of total deformation), which is minimal and does not significantly impact performance. It is also worth noting that the gripper rarely operates at such low pressures (around 25 kPa) in practical applications, where higher pressures align better with simulation results. Therefore, these minor discrepancies are within an acceptable range and do not affect the gripper's functionality under normal working conditions.

In summary, while finite element simulations serve as a valuable tool for predicting the behavior of the gripper, discrepancies between simulation and experimental results can arise due to factors such as material property variations, simplified geometrical assumptions, boundary condition differences, and experimental measurement uncertainties. The overall trends and behaviors observed in the experiments align well with the simulated predictions.

Figure 19 illustrates the operation of the flexible gripper as it engages with various objects using both positive and negative pressure modalities. The automation of the air pathway is managed by the Raspberry Pi GPIO, which modulates the solenoid valve, subsequently controlling the relay to actuate the valve's opening and closure. Upon activation of the air pump, depicted in Figure 19(a), the pressure within the inflatable palm increases, causing the adapter to extend in a specified direction. This mechanism effectively enhances the gripping range, achieving a dynamic radius between 4 cm and 7 cm. Notably, the maximum displacement of the inflated palm is observed at the middle lateral position, corroborating the findings from the simulation phase. For the empirical evaluation of the gripper's dexterity, two distinct objects were used: a 500-gram grapefruit with an 11 cm diameter and a 9 cm-radius pot, represented in Figures 19(b) and (c), respectively. The former assesses the gripping strength, while the latter demonstrates the internal support capabilities under negative pressure. Displacement measurements of the inflated finger reveal that peak displacement occurs at the fingertip in both pressure scenarios. The experimental results align closely with theoretical predictions, thus validating the effectiveness of the designed flexible gripper.

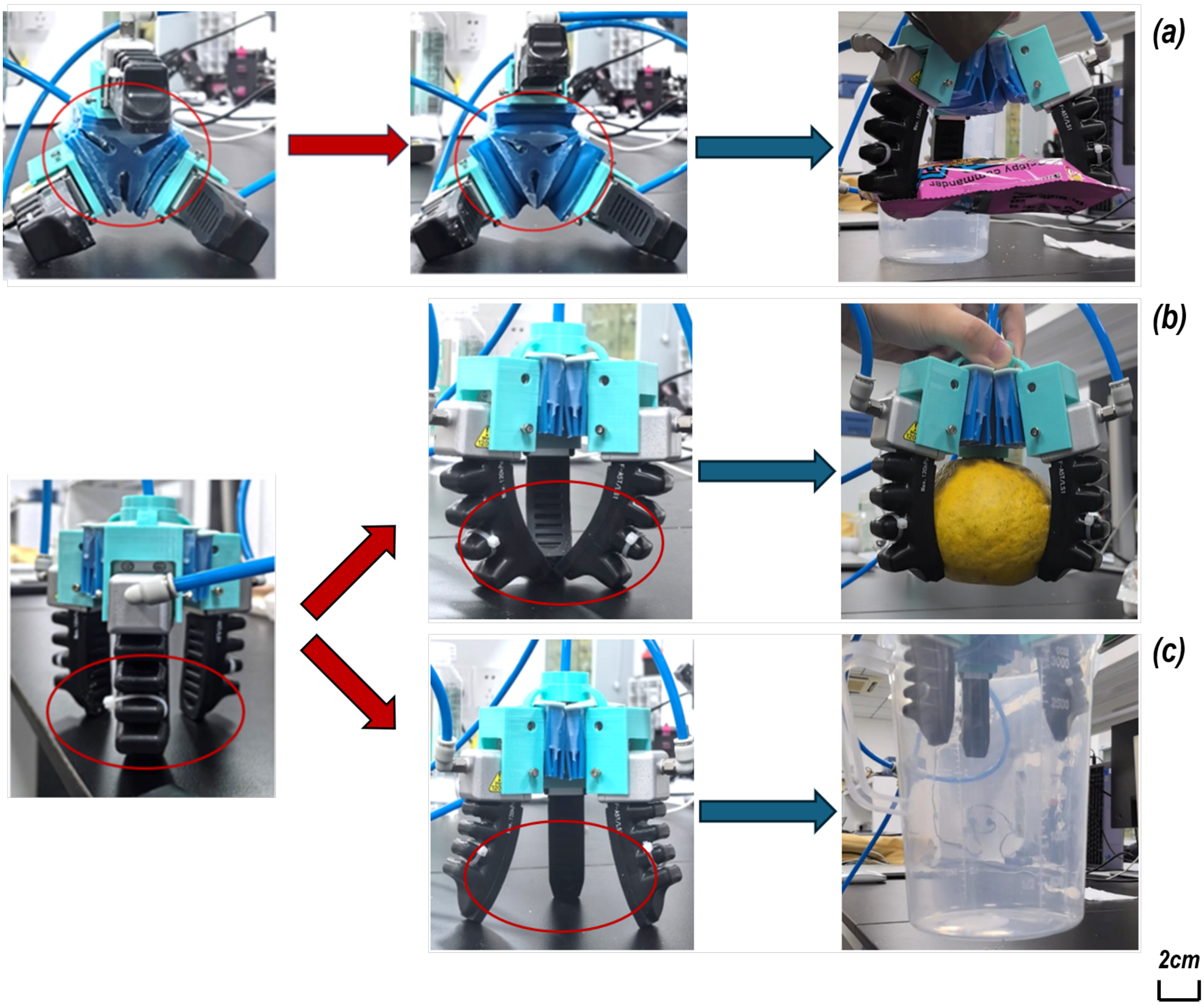

Figure 19. Preliminary tests for flexible gripper. **(a)** Case 3: Grasp an object using both the first expansion and second expansion, **(b)** Case 1: Grasp an object without using the expansion, **(c)** Case 4: Grasp an object using only the second expansion (Support an object internally).

Table 5 categorizes the objects grasped by Three-dimensional data, shape, mass, hardness and the required grasping radius. For instance, the table lists objects ranging from a flattened instant noodle bag to a granular spherical glutinous rice ball, covering a variety of shapes such as spherical, cup-shaped, and flattened. The masses of these objects vary from as light as 50 grams to as heavy as 800 grams. They also have different 3D data and Shore hardness. The grasping radius needed for these objects also spans from 45 mm to 65 mm, demonstrating the gripper's ability to adjust its grip based on the size and shape of the object.

Table 5. Experimental grasping results for different sizes and hardnesses of objects.

Grasping result	Target object name	Three-dimensional data(cm)	Shape type	Mass(g)	Shore hardness	Grasping radius range(mm)
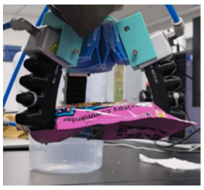	Instant noodle bag	$12 \times 12 \times 5$	Flattened	110	Shore A 30	65
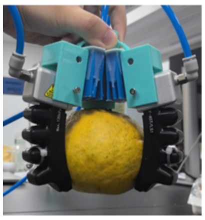	Grapefruit	5.5 cm-radius	Spherical	500	Shore A 20	55
	Bucket	9 cm-radius	Cup-shaped	50	Shore D 40	55
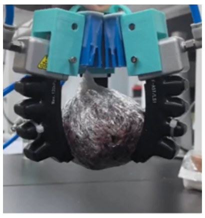	Sticky rice ball	4 cm-radius	Granular spherical	800	Shore A 10	45

4. Conclusion

This paper details the development of an novel flexible gripper that features an adjustable dynamic grasping range. In contrast to traditional methods that necessitate manual adjustments, our design utilizes a pneumatic inflatable palm, allowing for precise modulation and expansion of the grasping range, significantly enhancing the gripper's dexterity and overall grasping performance. We introduce a two-step expansion algorithm tailored to facilitate more accurate control of this range. Although the design is currently hindered by challenges such as the limited durability of 3D-printed materials and the non-homogeneous thickness of the silicone-based palm, experimental results underscore the effectiveness and practicality of the proposed gripper design.

Acknowledgment

This research has been supported in part by the Xi'an Jiaotong-Liverpool University (XJTLU) Teaching Development Fund under Grants TDF20/21-R22-144 and TDF22/23-R25-198, and in part by the XJTLU Research Development Fund under Grants RDF-22-01-081 and XJTLU Research Enhancement Fund under Grants REF-21-02-001.

Author's contribution

Conceptualization, methodology, validation, formal analysis, data curation, writing—original draft preparation—Jingxiang Wang, Yangzesheng Lu, Chengqi Song, Bingjie Xu; writing—review and supervision—Qinglei Bu, Jie Sun, Quan Zhang. All authors have read and agreed to the published version of the manuscript.

References

[1] Wang J, Lu Y, Song C, Xu B, Bu Q, *et al.* Design of Flexible Gripper with Inflatable Palm for Dynamic Grasping Range. In *2024 29th International Conference on Automation and Computing (ICAC)*, Sunderland, UK, August 28–30, 2024, pp. 1–7.

[2] Lu Y, Liu Y, Bu Q, Lim EG, Devaraj R, *et al.* An Autonomous Vehicle Platform for Parcel Delivery. In *2023 28th International Conference on Automation and Computing (ICAC)*, Birmingham, UK, August 30–September 1, 2023, pp. 1–7.

[3] Liu Y, Lu Y, Peng C, Bu Q, Liang YC, *et al.* Autonomous Vehicle Based on ROS2 for Indoor Package Delivery. In *2023 28th International Conference on Automation and Computing (ICAC)*, Birmingham, UK, August 30–September 1, 2023, pp. 1–7.

[4] Sun M, Xiao J, Lim EG, Zhang B, Zhao Y. Fast Template Matching and Update for Video Object Tracking and Segmentation. In *Proceedings of the IEEE/CVF Conference on Computer Vision and Pattern Recognition (CVPR)*, Seattle, USA, June 13–19, 2020, pp. 10791–10799.

[5] Sun M, Xiao J, Lim EG, Zhao C, Zhao Y. Unified Multi-Modality Video Object Segmentation Using Reinforcement Learning. *IEEE Trans. Circuits Syst. Video Technol.* 2024, 34(8):6722–6734.

[6] Sun M, Xiao J, Lim EG, Zhao Y. Starting Point Selection and Multiple-Standard Matching for Video Object Segmentation With Language Annotation. *IEEE Trans. Multimedia* 2023, 25:3354–3363.

[7] Li K, Xu Y, Zhao Z, Li A, Meng MQH. Closed-Loop Magnetic Manipulation for Robotic Transesophageal Echocardiography. *IEEE Trans. Robot.* 2023, 39(5):3946–3959.

[8] Kurundkar S, Kshirsagar K, Kulkarni V, Lambat H, Lambe M. 3D Printed Robotic Arm using Hand Gestures. In *2023 7th International Conference on I-SMAC (IoT in Social, Mobile, Analytics and Cloud) (I-SMAC)*, Kirtipur, Nepal, October 11–13, 2023, pp. 1087–1094.

[9] Koban N, Çavli N, Doğan H, Benli E. 7 DOF Robotic Arm Inverse Kinematic Analysis with Cuckoo and Whale Algorithms. In *2023 Innovations in Intelligent Systems and Applications Conference (ASYU)*, Sivas, Turkiye, October 11–13, 2023, pp. 1–5.

[10] Al Mhdawi AK, Wright N, Humaidi AJ, Azar AT. Adaptive PI-Fuzzy Like Control of a Stack Pneumatic Actuators Testbed for Multi-Configuration Small Scale Soft Robotics. In *2023 International Conference on Manipulation, Automation and Robotics at Small Scales (MARSS)*, Abu Dhabi, United Arab Emirates, October 09–13, 2023, pp. 1–8.

[11] Yiyang H. Design and fabrication, simulation test and application investigation of a new pneumatic soft actuator. Master's thesis, Hunan University, 2019.

[12] Gonzalez J, Poza J, Robles J, Ponce H, Brieva J, *et al.* Design of a Soft Gripper Hand for a Quadruped Robot. In *2023 IEEE 15th International Symposium on Autonomous Decentralized System (ISADS)*, Mexico City, Mexico, March 15–17, 2023, pp. 1–6.

[13] Gulnergiz ET, Dilibal S, Gormus B, Danquah JO, Emon OF. Additively Manufactured Soft Pneumatic Gripper Integrated Remotely Operated Underwater Vehicle (ROV) for Grasping Archeological Remains. In *2023 5th International Congress on Human-Computer Interaction, Optimization and Robotic Applications (HORA)*, Istanbul, Turkiye, June 08–10, 2023, pp. 01–05.

[14] Heeringa W, Santina CD, Smit G. FinFix: A Soft Gripper With Contact-Reactive Reflex for High-Speed Pick and Place of Fragile Objects. In *2023 IEEE International Conference on Soft Robotics (RoboSoft)*, Singapore, April 3–7, 2023, pp. 1–7.

[15] Shize Y, Zhouyi W, Zhendong D, Bingcheng W, Yu G, *et al.* Design of a bionic flexible robotic arm for aerospace requirements. *Mech. Manuf. Autom.* 2020, 49(1):134–137.

[16] Yoder Z, Macari D, Kleinwaks G, Schmidt I, Acome E, *et al.* A soft, fast and versatile electrohydraulic gripper with capacitive object size detection. *Adv. Funct. Mater.* 2023, 33(3):2209080.

[17] GitHub - SkyentificGit/SmallRobotArm: This is the open source project of the 6DoF robot arm based on stepper motors. Available: https://github.com/SkyentificGit/SmallRobotArm (accessed on 17 March 2024).

[18] Jain S, Dontu S, Teoh JEM, Alvarado PVY. A multimodal, reconfigurable workspace soft gripper for advanced grasping tasks. *Soft Robot.* 2023, 10(3):527–544.